Postprint of: Smakosz Ł., Tejchman-Konarzewski A., Evaluation of strength, deformability and failure mode of composite structural insulated panels, MATERIALS & DESIGN, Vol. 54 (2014), pp. 1068-1082, DOI: 10.1016/j.matdes.2013.09.032

EVALUATION OF STRENGTH, DEFORMABILITY AND FAILURE MODE OF COMPOSITE STRUCTURAL INSULATED PANELS

Ł. Smakosz and J. Tejchman

Faculty of Civil and Environmental Engineering

Gdańsk University of Technology

Narutowicza 11/12, Gdańsk 80-233, Poland

Phone: +48-58-347-14-81

e-mails: luksmako@pg.gda.pl, tejchmk@pg.gda.pl

Abstract

Composite structural-insulated panels (CSIPs) are novel prefabricated elements for structural applications. They are made from glass-fiber reinforced magnesia cement boards as facesheets and expanded polystyrene foam (EPS) as a core. The main aim of the paper is to present experimental results on the strength, deformability and failure mode of panels. Quasi-static full-scale and model tests under monotonic loading were performed to recognize mechanical properties of CSIPs. In the case of full-scale tests, bending and compressive, impact resistance, resistance to vertical and horizontal hanging loads and gradient temperature tests were carried out. In addition, compressive, shear and flexural small-scale tests were performed. The experimental results showed that CSIPS overcame several deficiencies of traditional structural insulated panels (SIPs). Some finite element modelling results within linear elasticity were also attached.

Keywords: composite structural-insulated panels, deflection, experiment, monotonic load, strength

NOMENCLATURE

A_s – service area [mm^2],

b – panel width [mm],

b_f – facesheet width [mm],

d – panel thickness [mm],

e – force eccentricity [mm],

E_f – modulus of elasticity of facesheet [N/mm^2],

E_c – modulus of elasticity of EPS [N/mm^2],

G_c – shear modulus of EPS [N/mm^2],

H – height [mm],

I – area moment of inertia of about neutral axis [mm^4],

l – distance between the supports [mm],

L – total panel length [mm],

M_u - ultimate bending moment [kNm],

p – pressure [kPa],

p_u – ultimate pressure [kPa],

P – vertical (horizontal) force [kN],

P_u – ultimate vertical (horizontal) force [kN],

P_{eq} – equivalent buckling force [kN],

t_c – core thickness [mm],

t_f – facesheet thickness [mm],

T – temperature [^{o}C],

u – displacement (deflection) [mm],

y – distance to the neutral axis [mm],

ε - normal strain [%],

ν – Poisson's ratio [-],

σ – normal stress [MPa],

σ_u – ultimate horizontal normal stress [MPa],

σ_u^f – ultimate horizontal normal stress in facesheet [MPa],

σ_u^c – ultimate horizontal normal stress in EPS core [MPa],

$\sigma_{10\%}$ – normal stress at 10% strain [MPa],

τ – shear stress [MPa],

τ_u – ultimate shear stress [MPa],

τ_u^c – ultimate horizontal normal stress in EPS core [MPa].

1. Introduction

The structural design in housing can be improved through the development and application of composite elements that capitalize on multifunctional components [1]. Structural insulated panels (SIPs), developed nearly 75 years ago, are high-performance 3-layered composite building panels used as elements in floors, walls and roofs of steel or wooden frameworks for

residential and light commercial buildings [2], [3]. These panels are fabricated in a factory and shipped to a construction site, where they can be quickly assembled to form a tight, energy-efficient building envelope. SIPs are simple composite sandwich panels formed as 3-layered constructions by bonding a thin layer (facing) to each side of a thick layer (core). Facesheets carry the bending stresses while a core resists the shear loads and stabilizes the faces against buckling and wrinkling. The core, that has lower mechanical properties compared to those of facesheets, increases the structure stiffness by holding the facesheets apart at a constant distance. The final product is light and has enhanced and more desirable properties than its constituents and possess a high stiffness-to-weight ratio. The most common facing material used in SIPs is the oriented strand board (OSB) (engineered wood product made from cross-oriented layers of thin, rectangular wooden strips compressed and bonded together with wax and resin adhesives [2]). Because it is a wood-based material, it requires a proper impregnation in order to prevent water infiltration, penetration resistance against wind borne debris and biological degradation (mould build-ups, termite attack). The SIPs' flexibility, strength and energy performance made them an important twenty-first-century building material for high-performance buildings in spite of some disadvantages [2].

In this paper, we investigated the last generation of prefabricated sandwich panels [4], [5] recently applied in building structures, called composite structural insulated panels (CSIPs) [2], [6], which overcome several problems of SIPs since they carry many added benefits. CSIPs are characterized by a higher strength to weight ratio and lower skills required for field construction. They are also fire resistant, waterproof and resistant to biological degradation in contrast to traditional SIPs. They are significantly stronger to both static and impact loads and have a higher facesheet/core stiffness ratio. They can be used for different elements in the structure, including structural elements (e.g. roofs and floors) and non-structural elements (e.g. non-load bearing walls and partitions) [6]-[8].

CSIPs considered in this paper are made from thin glass-fiber reinforced magnesia cement boards (called also magnesium oxide boards) as facesheets and thick expanded polystyrene foam (EPS) as a core, both connected by a thin adhesive layer (Fig.1). These CSIPs were developed 5 years ago in USA and introduced in 2010 into the Polish building market by the Polish building company LS TECH Homes. The wall panel dimensions are $0.174 \times 1.0 \times 2.5$ m^3 and their overall mass is 70 kg. Unfortunately, the high stiffness-to-mass ratio of CSIPs results in a low level of the sound insulation due to the appearance of resonant frequencies in the EPS core – this disadvantage has to be removed [9]. In addition, their intrinsic anisotropy, non-homogeneity and

complex failure mechanisms (e.g. yielding of facesheet in tension, core shear failure, core crushing, global buckling, debonding, delamination) cause that their correct and reliable static design is extremely difficult.

Our paper is mainly experimentally oriented. The aim of the present research work is to describe some important mechanical properties of CSIPs and their constituents (EPS, glass-fiber reinforced magnesia cement boards) under flexural, compressive and tensile quasi-static monotonic loads. Comprehensive standard and non-standard laboratory tests were performed on natural-size and small-size specimens at Gdańsk University of Technology. Flexural full-scale tests were performed with 2.50 m long, 1.0 m wide and 0.174 m thick panels and full-scale compressive tests were carried out with 2.75 m long, 1.0 m wide and 0.174 m thick panels. Based on laboratory tests, the main strength properties of panels for an engineering design were determined. In addition, some finite element modelling results within linear-elasticity were attached. Both, the experimental results of dynamic, impact and fatigue experiments on single panels and panels' joints and the outcomes of finite element calculations based on elasto-plasticity in a hardening regime for EPS and facesheets and cohesive crack zones [10] in a softening regime for EPS, facesheets and interface zones will be published in the next paper.

Our main research intention is to use CSIPs as load bearing elements together with fiberline pultrusion structural profiles in residential buildings based on comprehensive laboratory tests and finite element calculations. Our experimental study described in this paper may contribute to a design a new type of residential buildings by taking into account mechanical properties of CSIPs. Heat and acoustic problems of CSIPs will be also taken into account [9].

2. Facesheet and core material

Figure 1 presents the cross-section of a single CSIP. The facings, made from magnesia cement boards, are composed mainly of magnesium oxide, magnesium chloride, perlite, wood fiber and reinforced with a fiberglass mesh (Fig.2). The boards are a composite whose properties depend strongly on a production process, thickness, number and placement of glass-fiber meshes. This means that even similarly looking boards may vary in properties. The magnesia cement boards have better mechanical properties than the OSB boards, they are fireproof, waterproof, durable, resistant to fungus and insects and have smoother external surfaces. However, they require a strict fabrication process control. Otherwise, they may be subjected to fast degradation due to the water infiltration and freezing-thawing processes.

The external magnesia cement boards used in CSIPs considered in the paper were 11 mm thick and reinforced with two layers of glass-fiber mesh (mass density 900 kg/m^3) (Fig.2). The core of the analysed CSIP is made from the expanded polystyrene (EPS) – the light-weight, rigid and tough closed-cell foam commonly used as a thermal insulation building material. Its mechanical properties have an immense influence on the overall flexural stiffness of the panel and are strongly dependent upon its mass density. The EPS core used in CSIPs considered in the paper was 152 mm thick and its mean mass density was 20 kg/m^3.

3. Experimental set-ups

3.1 Large-scale tests

The mechanical tests on CSIPs of Fig.1 were performed in accordance with recommendations by ETAG 016 [11]. All tests (Tab.1) were carried out with panels of a different length under the displacement control.

First, two flexural tests were conducted on the simply-supported wall panel 2500×1000×174 mm^3 under uniform pressure corresponding to wind and snow (Fig.3a). The distance between the supports was l=2200 mm and the service area was A_s=2200×1000 mm^2 (Fig.3b). The pressure load was simulated by four the same line forces (at the equal distance) along the panel width prescribed to steel elements put on rubber pads. The forces were in a normal direction to the surface top throughout the entire experiment owing to the use of hinges in the load system. Two panels of the same geometry were tested with two different deflection rates (0.1 mm/min and 3.0 mm/min). The deflection at the mid-span and the total vertical force were always registered.

Next, three connected panels forming the wall 3 m wide were tested (1 test) under bending with the deflection velocity of 0.5 mm/min (Fig.4a) with l=2200 mm and A_s=2200×1000 mm^2 (Fig.4b). The deformation was prescribed to the mid-panel. The panels were connected by two OSB splines inserted into slots in the core and fixed with screws.

Later, the flexural tests on a single wall panel and 3 connected wall panels fixed on supports by means of screws (2 tests) were performed under the deflection velocity of 0.5 mm/min (Figs.5 and 6) with l=2500 mm and A_s=2500×1000 mm^2 (Fig.5b). Such fixing was to simulate a connection of wall panels with foundations or floors. The fiberline structural profiles were

inserted into core slots along the short panel edge, sealed with the mounting foam and connected with a stiff supporting frame by connectors. Two rows of two screws were at 1/3 and 2/3 of the height along one support end (4 screws in total) and one screw at the mid-height along the second support edge.

The soft body impact test simulating a possible person accident against a wall [9] was performed with a three panels' wall fixed to a stiff frame (Fig.7). The experiment was done in order to check the safety in use and serviceability to determine whether the wall can prevent penetration by a falling weight and if it can be used after the impact. A 50 kg bag containing 2-4 mm aggregate, 400 mm in diameter, hanging on a rope under the angle of 65^{o} was used as an impactor in both cases. In the safety case, a single drop from the height of 1.8 m was executed resulting in the impact energy of 900 Nm. In turn, in the serviceability case, three drops at the height of 0.8 m were done resulting in the impact energy of 400 Nm.

The hard body impact test (Fig.8) was carried out to simulate a hard object hitting centrally a wall panel [11]. In the safety case, a steel ball with the diameter of 63.5 mm and mass of 1 kg was dropped at the distance of 1.02 m resulting in the impact energy of 10 Nm. In the serviceability case, the 0.5 kg steel ball with the diameter of 50 mm was dropped three times at the distance of 1.22 m on the same spot (the impact energy was 6 Nm). The tests were performed with a simply-supported wall panel (Fig.8).

The thermal test [11] included a gradual uniform heating of the panel top up to the temperature of 80ºC while keeping the panel bottom at the constant temperature of 23ºC. The experiment consisted of two phases (Fig.9). In the first phase, the panel curvature radius was measured with its short edges fixed to a stiff frame. In the second phase, a support was added and the deflection at the ¼ and ¾ of the span and reaction force at the mid-support were measured.

In addition, the facesheet strength test against a pull-out force [11] caused by objects fixed in a parallel and perpendicular direction to the facing surface was also conducted (Fig.10).

Finally, three wall panel compression tests were carried out under the axial and eccentric load (Fig.11). The dimensions of three tested panels were $2750\times1000\times174$ mm^3 and the compressive force eccentricity was $e=0$, $e=d/6$ and $e=d/3$ (d=174 mm – the panel thickness). Due to technical limitations, the tests were performed in a horizontal orientation with both ends supported on hinges (Fig.11). In order to obtain relatively uniform distribution of stresses at ends, the panels

were inserted into steel profiles and sealed with concrete (Fig.12) or polyurethane foam (PUR). The steel profiles had the height of 165 mm and the total distance between the support points was 3080 mm. The horizontal displacement velocity was 4 mm/h.

3.2 Small-scale tests

The tests were carried out with specimens of CSIPs, EPS and glass-fiber magnesia cement boards (Tab.2). The specimens were cut out from two panels coming from two various product batches.

The flatwise compression, tension and three-point bending experiments (4+4+8 tests, respectively) were performed for EPS according to [12]-[14] in order to determine the Young's modulus, yield stress and nonlinear behaviour of EPS in a direction perpendicular to the panel plane. The specimen size under compression and tension was 100×100×152 mm^3. Long beams with the thickness of 150 mm, width of 100 mm and span of 1300 mm and short beams with the thickness of 75 mm, width of 100 mm and span of 650 mm were used. In order to measure the shear strength and shear modulus, a doubled specimen 50×100×200 mm^3 was used (2 tests) [15].

The glass-fiber-reinforced magnesia cement boards were tested in compression on the specimens of 11×50×50 mm^3 (8 tests) and under three-point bending [16] (8 tests) with the specimens 11 mm thick, 100 mm wide at the support span of 360 mm. As glass-fiber reinforcing mesh has a different layout in a direction of the panel length (called production line direction – straight stretched fibers) and in a direction perpendicular (loose fibers). The tests were conducted on samples cut out in these two directions.

With respect to specimens of CSIPs, the edgewise compression tests were performed based on ASTM: C364/C364M-07(2012) and [6]. Three types of specimens were used (Fig.13): one possessing the wall panel cross-section (200×174×750 mm^3) and two with the reduced core thickness (40×100×275 mm^3 and 45×100×650 mm^3). In total, 6 tests were carried out. In three-point bending tests (based on ASTM: C393/C393M-11e1), the thickness and width of specimens were 174 mm and 100 mm at the different beam span (the distance between supports was 275 mm, 600 mm and 1250 mm, respectively). In total, 12 tests were carried out.

4. Experimental results

4.1 Large-scale tests

The experimental results of bending tests on simply-supported wall CSIPs of Figs.3 and 4 are presented in Fig.14. The behaviour of panels under the uniform static load was linearly elastic up to the peak (Figs.14IA and 14IIA). After the peak, it was brittle. The single panel and panels' wall failed both due to cracking at the lower facesheet. The effect of loading velocity was rather negligible. The ultimate vertical force was very high: for a single wall panel P_u=20.1-20.9 kN at the deflection u=17-19 mm (which corresponded to the maximum uniform load pressure of $p_u=P_u/A_s$=9.1-9.5 kN/m^2) and for 3 panels' wall more than twice – P_u=46 kN at u=24 mm (corresponding to the maximum uniform pressure of $p_u=P_u/A_s$=20.9 kN/m^2). The lower facesheets failed when the horizontal normal stress was exceeded of σ_u^f=4.0 MPa based on the measured ultimate normal strain ε_u=0.065-0.070% (Figs.14IB and 14IIB) with E_f=5716 GPa. In turn, the ultimate normal stress obtained from the usual beam theory is by 15% smaller: σ_u=3.3-3.7 MPa ($\sigma_u=(M_u y)/I$, where M_u - the ultimate bending moment, y=87 mm - the facesheet distance to the neutral axis and $I=2[t_f^3 b_f/12+b_f t(t_f/2+t_c/2)]=2.927\times10^8$ mm^4 – the area moment of inertia of facesheets about the neutral axis (t_f – the facesheet thickness, b_f – the facesheet width and t_c – the core thickness).

The experimental results for wall panels fixed on supports by means of screws are presented in Fig.15. Up to the peak, the panels behaved non-linearly due to a sparse number of screws. The ultimate vertical force for a single wall panel was P_u=12 kN at u=28 mm (which corresponded to the ultimate pressure of $p_u=P_u/A_s$=4.8 kN/m^2=4.8 kN/m^2) and for a wall composed of 3 connected panels again more than twice P_u=29 kN at u=40 mm (corresponding to the ultimate uniform pressure of p=11.6 kN/m^2). The failure mechanisms were similar as at simply-supported wall panels – the lower facesheet first failed at the normal strain of ε_u=0.070-0.075% (σ_u^f=4.3 MPa). One difference was the appearance of a discrete crack on the upper facesheet near the support in the test with a wall of 3 panels due to the bending support moment (Fig.15B). The maximum normal stress from the usual beam theory is again smaller: σ_u=2.3-2.7 MPa.

Both, the impact of a soft and a hard body of Figs.7 and 8 left only insignificant penetration and damage traces on the panel surface. Thus, both the serviceability and safety of panels against impacts was satisfied. In the thermal results for a wall panel of Fig.9, the curvature radius was 320 m (in the first experimental phase), and the deflection was 0.5 mm and the reaction force

680 N at the mid-support (in the second experimental phase). Thus, the effect of the gradient temperature on the panel deformation was negligible (the panel deflection was 0.08% of the span between the fixed points only). In the facesheet strength tests against a force caused by objects fixed to a facesheet (Fig.10), the ultimate normal force was 1.7 kN and the ultimate shear force was 2.5 kN. The facesheet damage had a local character only.

The results of compressive tests for wall panels of Fig.11 with 3 different eccentricities e are described in Figs.16 and 17. The maximum horizontal forces P for tested wall panels were P_u=131 kN (e=0 mm), P_u=197 kN (e=d/6) and P_u=163 kN (e=d/3) at the horizontal displacement u=12-18 mm, respectively (d=174 mm – the panel thickness). The ultimate vertical normal stress was calculated from the usual formula for eccentric compression $\sigma_u(y)=P_u/A+P_u e\ y/I$=6.1-12.7 MPa. The force-displacement relationship was linear ($e\neq$0 mm) or non-linear (e=0 mm) up to the peak. After the peak, the panel behaviour was brittle ($e\neq$0 mm) or quasi-brittle (e=0 mm). The unexpectedly low strength of the axially loaded panel was probably caused by a weak strength quality of facesheets. No local or global buckling, debonding or delamination took place. The damage was always initiated (e=0 and e=d/6) by fracture of a facesheet within a steel 'C' profile surrounding the panel (Fig.12) leading to its splitting and the formation of a large gap between the panel and steel profile (Fig.17a). At e=d/3 when PUR was used as the fill, an abrupt break of the panel beyond the steel profile occurred (Fig.17b). The global moduli of elasticity E were equal to 2530 MPa (e=0 mm), 2570 MPa (e=d/6) and 1670 MPa (e=d/3) (Fig.16). For e=0 the normal strains on the facesheet top and bottom measured in the moment of sample failure were -0.11% and -0.16%, respectively, causing the normal stress σ=2.8-4.0 MPa. In the case of e=d/6, the bottom and top normal strains in the faceesheet were -0.32% and -0.12% (σ=3.1-8.2 MPa) and at e=d/3, the bottom and top normal strains were -0.38% and 0.05% (σ=0.8-6.3 MPa). The normal stresses measured at the mid-span were lower than the ultimate stress calculated at the end by 34% (e=0), by 32% (e=d/6) and by 50% (e=d/3).

4.2 Small-scale test

EPS core

Figs.18 and 19 presents the flatwise compression and tension test results from single tests with EPS which are typical for foam materials. During compression, the initial part of the stress-strain diagram indicated a linear elastic behaviour at very low strain (up to 2%) (Fig.18). Next the material underwent hardening connected to the densification. This process was rather weak up to

strain equal to ε=70% and later became very strong since a cellular foam structure was completely crushed. The vertical normal stress was σ_u^c=0.11 MPa at the vertical normal strain ε=10% (E_c=6.09 MPa) (Tab.3). During tension (Fig.19), a brittle mode occurred due to the occurrence of a discrete tensile crack in a horizontal direction in the mid-region. Initially, the material behaviour was linear, later non-linear up to the peak. The maximum vertical normal stress was on average σ_u^c=0.22 MPa at ε=3.5% (E_c=10.37 MPa), Tab.3. The evolution of experimental curves from three-point bending tests (Fig.20) and a failure mechanism were similar as in tension (Fig.19). The maximum vertical normal stress was on average σ_u^c=0.20 MPa at ε=2.4% (E_c=8.01 MPa), Tab.3. During shearing (Fig.21), the material indicated a non-linear behaviour before and after the peak. The ultimate shear stress during was on average τ_u^c=0.22 MPa with G_c=2.51 MPa (Tab.3).

Magnesia cement facesheets

The typical uniaxial compression and three-point bending test results with the facesheet are shown in Figs.22 and 23. During compression and bending, the material behaviour was independent of the cutting direction The behaviour was linear up to the peak and quasi-brittle after the peak during compression (Fig.22a) and linear-non-linear up to the peak and brittle after the peak during bending (Fig.23a). The damage in the form of a vertical crack was initiated in the contact area with a loading plate during compression (Fig.22b) and initiated at the mid-section under the vertical force during bending (Fig.23b). The average modulus of elasticity of facesheets in a production line direction was E_f=1922 MPa (uniaxial compression) and E_f=5716 MPa (bending). During bending, it was 700 times higher than for EPS (E_c=8.01 MPa). The average ultimate stress for facesheets was σ_u^f=13.50 MPa in compression and σ_u^f=9.67 MPa in bending.

Our experimental results for the EPS core and facesheets are summarized in Tab.3. The quantities of E_c, G_c, σ_u^c, τ_u^c and $\sigma_{10\%}$ for EPS are in a satisfactory agreement with the comparative ones from the scientific literature [17]-[20] but the values of E_f and σ_u^f for facesheets are lower than in [21] (Tab.3).

CSIP specimens

The edgewise compression test results for different specimen geometries of Fig.13 are summarized in Fig.24. The global buckling was solely obtained in a very slender specimen with the reduced EPS thickness (Fig.24c). Other specimens failed through fracture and splitting of a facesheet (Figs.24a and 24b) - they showed no signs of debonding between constituents. The maximum vertical normal stress changed between 5.6-15.5 MPa at the vertical normal strain ε=0.2-0.6% (E=3414-3950 MPa).

The maximum compression force for the buckled sandwich specimen (Fig.24c) was compared with the analytical formula for the equivalent buckling force P_{eq} of CSIP under eccentric loading [6] that takes into account orthotropic facesheets and EPS core in terms of its thickness t_c and shear modulus G_c

$$P_{eq} = \frac{\pi^2}{(1+\frac{6e}{d})L^2} \frac{E_f I_f}{(1+\frac{\pi^2 E_f I_f (1-\nu_f{}^2)}{L^2 b(\frac{d+t_c}{2})G_c})} (1-\nu_f{}^2), \quad (1)$$

where E_f is the longitudinal modulus of elasticity of magnesia cement facesheets (MPa), ν_f - the Poisson's ratio of facesheets, G_c - the EPS shear modulus, b=100 mm - the panel width, d=174 mm – the panel thickness, L=955 mm - the panel length, t_c=152 mm – the core thickness and I_f – the moment of inertia of facesheets about the panel centroid. With the average material parameters in Tab.3 (with ν_f=0.20), the force P_{eq} in Eq.1 was 6.23 kN (e=0), i.e. twice smaller that the experimental buckling force.

Fig.25 shows the three-point bending test results. The longest beams failed by tension in the lower facesheet (Fig.25a), while two other short beams failed by the EPS core crushing under the loading points and the successive facesheet cracking (Fig.25c). The maximum vertical force was P_u=1.8-2.3 kN at the deflection u=15-28 mm. The maximum vertical normal stress changed between 2.50-3.63 MPa.

The experimental results show that the properties of CSIPs under bending and compression may be approximately determined with small-scale laboratory tests (thus some large-scale tests are not needed). The ultimate normal stress in bending σ_u can be determined with flexural tests on

composite beams, and the ultimate normal stress σ_u and modulus of elasticity E in compression with edgewise uniaxial compression tests on the facesheet material.

5. FE analyses

Some simplified numerical simulations were performed using the commercial FE program ABAQUS [22]. Isotropic linear-elastic material models for EPS and facesheets were assumed only. Both constituents were connected by perfect bond. The outcomes might be used for the engineering practice.

Simplified flexural test simulations of a large-scale wall panel and a small-scale beam were performed under plane stress conditions by taking the geometric linearity into account. The 4-node linear solid elements with the reduced integration and hourglass control were used. The element size was 2 mm resulting in 6 elements along the facesheet thickness and 76 elements along the core thickness. The symmetry axis was considered in large-test analyses. The material properties were taken based on the average test results from small-scale tests on separate constituents (Tab.3). Two different sets of material parameters were used: the data set '1' modulus of elasticity in bending for facesheets and EPS (Tab.3) and the data set '2' the modulus of elasticity in bending for the bottom facesheet, modulus of elasticity in compression for the top facesheet, modulus of elasticity in compression for the upper half of EPS and the modulus of elasticity in tension for the lower half of EPS (Tab.3). The FE calculations were performed until the maximum vertical force reached the experimental one.

The numerical results are compared with the experimental ones in Figs.26 and 27. The data set '1' provides a realistic result for the small-scale test only (Fig.26A). In contrast, the data set '2' is in a satisfactory agreement for both test types (Figs.26A and 26B). The calculated horizontal normal strain at the bottom facesheet (Fig.27) was equal to 0.159% (data set '1') and 0.156% (data set '2') in small-scale test simulations and 0.061% (data set '1') and 0.063% (data set '2') in large-scale test simulations. The latter results were by 10% smaller than the measured of 0.07%. In turn, the calculated horizontal normal stress at the bottom facesheet was equal to 8.39 MPa (data set '1') and 8.15 MPa (data set '2') in small-scale test simulations and 3.48 MPa (data set '1') and 3.78 MPa (data set '2') in large-scale test simulations.

Next, a 3D flexural test for 3 panels' wall was numerically simulated. The facesheets and OSB board splines connecting panels were modelled with 8-node continuum shell elements 6×15 mm^2

(2 elements along the facesheet thickness and OSB spline thickness). The core was modelled with 8-node solid elements 20×20×20 mm^3 with the reduced integration and hourglass control (8 elements along the core thickness). The connection between OSB splines and facesheets was realized as pairs of nodes tied together at the spacing of 480 mm. In turn, the connection between the core and OSB spline was as perfect bond. A quarter of the test specimen was computed. The material properties were the same as during simulations of a single CSIP. The modulus of elasticity of the OSB board was 2500 MPa (according to the product's specification). The calculations were again performed until the maximum vertical force reached the experimental one. The simulation results of Fig.28 indicate that the data set '2' provides again the more realistic FE results with respect to the experiments. However, the agreement is worse than in Fig.26 probably due to too simplified boundary conditions along the connection between OSB splines and facesheets.

Finally, some FE simulations were performed for two compression tests by taking the geometric linearity into account ($e=d/6$ in a large-scale test simulation and $e=0$ in a small-scale test simulation) (Figs.29). Rigid steel profiles used in experiments were modelled by assuming a normal contact interaction without friction along CSIP. In small-scale analyses, one steel profile was fixed and the other was supported as a hinge, and in large-scale analyses, the both steel profiles were taken at ends as hinges. Two sets of input material data were assumed for facesheets and core (Tab.3): the data set '1' with uniaxial compression properties and the data set '2' with flexural properties. The FE calculations were solely performed up to the top displacement of 10 mm in a large-scale test simulation and of 3 mm in a small-scale test simulation. The comparative results of Fig.29 show however a strong discrepancy between FE results and experiments (the calculated curves $P=f(u)$ indicate either too large or too small horizontal force P and stiffness). Thus, the assumed FE model with uniform linearly elastic material properties for facesheets and EPS (determined with uniaxial compression and bending tests) and simplified boundary conditions at CSIP's ends proved to be too simple to reproduce experiment results.

6. Discussion

Our experimental large-scale tests show that the general behaviour of CSIPs under loading is initially linear, then slightly non-linear and finally brittle at failure (Figs.14 and 16) except of panels under bending fixed on supports by means of a few screws which indicate a non-linear behaviour from the test beginning (Fig.15). For bending tests, the tensile failure of the bottom

facesheet always occurs [9]. In turn, for compression the failure occurs after the compressive strength of facesheets is reached (thus, global buckling never happens (Fig.16)). Thus CSIPs show at failure no debonding between constituents and no global buckling, no local buckling wrinkling of facesheets and no local EPS crushing which occur frequently in different composites sandwich constructions [6]. They are more advantageous than e.g. CSIPs with the EPS core and thin glass/polypropylene facesheets (t_f=3.04 mm) described in the references [6]-[8] which underwent global buckling.

The initial FE results show that a linear elastic approach with constituents connected by perfect bond is too simple to describe the behaviour of single CSIPs under compression and three connected CSIPs under bending (Figs.27-29). Thus, the more sophisticated numerical model is needed that takes into account the material non-linearity in a hardening regime, anisotropy, cracking process and interface layers between constituents [10]. For simply supported panels, the most realistic FE results are obtained when using elastic properties of constituents from compressive and bending tests respectively for top and bottom parts of the model. The flexural stiffness of panels in large-scale tests depends mostly on the core properties.

7. Conclusions

The following conclusions can be derived from our comprehensive laboratory quasi-static experiments and under monotonic loading at full- and small-scale and FE analyses with novel light composite structural insulated panels CSIPs for structural applications in residential buildings:

- The sandwich panels are a very attractive structural product from a mechanical and insulating point of view. Therefore, they are a good candidate product to replace the traditional structural insulated panels SIPs. At failure, they show no debonding between constituents, no local buckling of facesheets and no local EPS crushing. They have a great potential as load-bearing elements in buildings (roofs, floors and walls) with respect to their high strength.

- During bending, simply-supported wall panels may carry 9.1 kPa and simply-supported walls composed of 3 panels may even carry 20.9 kN/m^2 in a horizontal direction at the permissible horizontal displacement of 30-40 mm. If wall panels are fixed by means of screws, they can carry 4.8 kPa (single panel) or 11.6 kPa (3 connected panels). During compression, a hinged-

supported wall panel carries 458-788 kPa in a vertical direction at the permissible vertical displacement of 12-18 mm. At failure, the behaviour of CSIPs is brittle.

- The ultimate horizontal normal flexural stress based on the measured normal strains is 4.0 MPa in large-scale tests, and is higher that according to the usual beam theory: 2.5-3.6 MPa (small-scale tests) and 2.3-3.7 MPa (large-scale tests). In turn, the measured ultimate normal compressive stress is 8.4-18.3 MPa (small-scale tests) and 4.0-8.2 MPa (large-scale tests). The Young modulus in compression in small- and natural-scale tests is similar and ranges between 1453 MPa and 2610 MPa.

- The properties of magnesia cement facesheets may strongly vary in production batches (their strict quality control is thus desired). A special care should be paid to prevent damage of facesheet edges during transport and montage as it is the area wherein failure of composite panels always initiates.

- The PUR foam is recommended in the contact area between panels and rigid boundary steel or fiberline profiles in order to ensure a uniform stress distribution in facesheets.

- The bending and compression properties may be approximately determined with small-scale tests. The ultimate horizontal normal stress in bending can be determined by means of small flexural tests on CSIP specimens and the ultimate normal stress and modulus of elasticity in compression can be obtained with edgewise uniaxial compression of small facesheet specimens. In order to predict the deflection of single CSIPs under bending, a simplified FE model of two linearly elastic materials (facesheet and core) with mean compressive and bending properties from small-scale tests and the failure normal stress from small- and large-scale bending tests on CSIPs may be applied.

- In general, a linear elastic FE approach is too simple to describe the behaviour of CSIPs.

References

[1] Peters ST. Handbook of composites. London, Chapman & Hall; 1998.

[2] Report on Expanding the Scope and Market of SIP Technologies: A history of SIPs and CSIP manufacturing, construction and market issues. The Federation of American Scientists, 2009.

[3] Lstiburek J. Builder's Guide to Structural Insulated Panels (SIPs) for all Climates. Building Science Press, 2008.

[4] Zenkert D. An introduction to sandwich construction. West Midlands, United Kingdom: Engineering Materials Advisory Service Ltd.; 1995.

[5] Borsellino C, Calabrese L, Valenza A. Experimental and numerical evaluation of sandwich composite structures. Composites Science and Technology 2004, 64: 1709-1715.

[6] Mousa MA, Uddin N. Global buckling of composite structural insulated wall panels. Materials and Design 2011, 32: 766-772.

[7] Mousa MA, Uddin N. Flexural Behavior of Full-Scale Composite Structural Insulated Floor Panels. Advanced Composite Materials 2011, 20: 547-567.

[8] Mousa MA, Uddin N. Structural behavior and modeling of full-scale composite structural insulated wall panels. Engineering Structures 2012, 41: 320-334.

[9] Smakosz Ł, Wawrzynowicz A, Krzaczek M, Tejchman J. Experimental and numerical evaluation of composite structural insulated wall panels. Proc. 15th European Conference on Composite Materials ECCM 15, Venice, Italy, 24-28.06.2012.

[10] Tejchman J, Bobiński J. Continuous and discontinuous modeling of fracture in concrete using FEM. Springer Berlin-Heidelberg (Wu W, Borja RI, editors); 2013.

[11] EOTA. ETAG 016: Guideline for European Technical Approval of Self-Supporting Composite Lightweight Panels, 2003.

[12] EN 826:1998: Thermal insulating products for building applications - Determination of compression behaviour, 1998.

[13] EN 1607:1999: Thermal insulating products for building applications - Determination of tensile strength perpendicular to faces, 1999.

[14] EN 12089: 2000: Thermal insulating products for building applications - Determination of bending behaviour, 2000.

[15] EN 12090: 2000: Thermal insulating products for buildings applications - Determination of shear behaviour, 2000.

[16] EN 12467: 2009: Fibre-cement Flat Sheets - Product Specification and Test Methods, 2009.

[17] Gnip IY, Vejelis S, Kersulis VI, Vaitkus S. Deformability and strength of expanded polystyrene (EPS) under short-term shear loading. Mechanics of Composite Materials 2007. 1: 85-94.

[18] Gnip IY, Vejelis S, Kersulis VI, Vaitkus S. Deformability and tensile strength of expanded polystyrene under short-term loading. Polymer Testing 2007, 26: 886–895.

[19] Gnip IJ, Vaitkus S, Kersulis VI. Deformability of expanded polystyrene under short-term compression. Mechanics of Composite Materials 2007, 43, 5: 433-444.

[20] Vėjelis S, Vaitkus S. Investigation of bending modulus of elasticity of expanded polystyrene (EPS) slabs. Materials Science 2006, 12, 1: 22-24.

[21] www.framecad.com.

[22] ABAQUS, Standard User's Manual Ver. 6.10, Hibbitt, Karlsson & Sorensen, Inc. 2011.

LIST OF FIGURES

Fig.13: Specimens of CSIPs used in edgewise compression tests: a) with wall panel cross-section, b) with low slenderness ratio at reduced EPS thickness, c) with high slenderness ratio at reduced EPS thickness

Fig.14: Bending tests with simply-supported wall CSIPs: I) single wall panel, II) three-panels' wall, A) vertical force P versus deflection u at two different deflection velocities 0.1 mm/min (panel 'a') and 3 mm/min (panel 'b'), B) vertical force P versus normal strain at mid-span ε (a1 and a2 – panel bottom, b1 and b2 – panel top, c1 – mid-panel bottom, c2 – mid-panel top), C) panel's failure mode

Fig.15: Bending tests with wall CSIPs fixed on supports by means of connectors: A) vertical force P versus deflection u for single panel, B) vertical force versus deflection for wall of three connected panels and wall at failure (view on top surface)

Fig.16: Compression tests with wall CSIPs: A) horizontal force P versus horizontal edge displacement u at 3 different eccentricities e (d – panel thickness), B) horizontal force P versus horizontal normal strain ε at mid-span with e=0 (1 – bottom, 2 - top), C) horizontal force P versus horizontal normal strain ε at mid-span with $e=d/6$ (1 - bottom, 2 – top), D) horizontal force P versus horizontal normal strain ε at mid-span with $e=d/3$ (1 - bottom, 2 – top)

Fig.17. Failure mechanism in compressive tests on CSIPs: a) specimens sealed with concrete (e=0 and $e=d/6$) and b) specimens sealed with PUR foam ($e=d/3$)

Fig.18: Flatwise compression test with EPS (size 100×100×152 mm^3): A) vertical normal stress σ - vertical normal strain ε curve, B) specimen before (a) and after test (b)

Fig.19: Flatwise tension test with EPS (size 100×100×152 mm^3): a) vertical normal stress σ - vertical normal strain ε curve, b) specimen after failure

Fig.20: Three-point bending test with EPS a) size 75×100×650 mm^3, b) size150×100×1300 mm^3): A) normal stress σ – deflection u curve, B) specimen after failure

Fig.21: Shear test with EPS (50×100×200 mm^3): a) vertical force P – vertical displacement u curve, b) specimen after failure

Fig.22: Compression test with magnesia cement boards (11×50×50 mm^3): a) vertical force P – vertical displacement u curve, b) failure mode

Fig.23: Three-point bending test with magnesia cement board specimens (11×100×360 mm^3): a) vertical force P - deflection u curve, b) specimen failure

Fig.24: Compression test with CSIPs of Fig.12: A) vertical normal stress σ - vertical normal strain ε curves and B) failure modes for specimens with: a) real panel cross-section 200×174×750 mm^3, b) low slenderness ratio at reduced EPS thickness 40×100×275 mm^3 and c) high slenderness ratio at reduced EPS thickness 45×100×650 mm^3

Fig.25: Three-point bending test with CSIPs of Fig.12: A) vertical force P - deflection u curves and B) failure mode for specimens with span between supports: a) 275 mm, b) 600 mm and c) 1250 mm

Fig.26: Bending results for CSIPs: vertical force P versus deflection u in large-scale panel test (A) and small-scale test (B), a) experiments, b) FEM (data set '1'), c) FEM (data set '2')

Fig.27: Distribution of horizontal normal strain on deformed CSIPs specimens under bending: a) large-scale test (specimen half was modelled), b) small-scale test (entire specimen was modelled)

Fig.28: Bending results for three-panel's wall: vertical force P versus deflection u: a) experiments, b) FEM (data set '1'), c) FEM (data set '2')

Fig.29: Compression results for CSIPs: horizontal force P versus horizontal support displacement u in large-scale panel test (A) and small-scale test (B), a) experiments, b) FEM (data set'1'), c) FEM (data set '2')

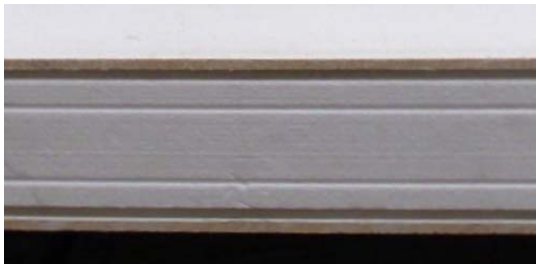

a)

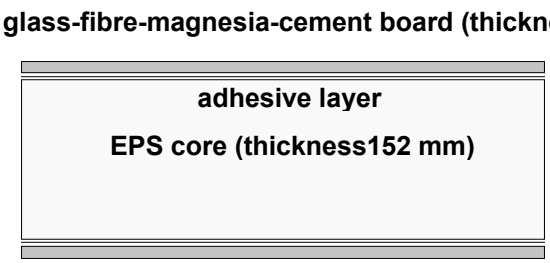

b)

FIGURE 1

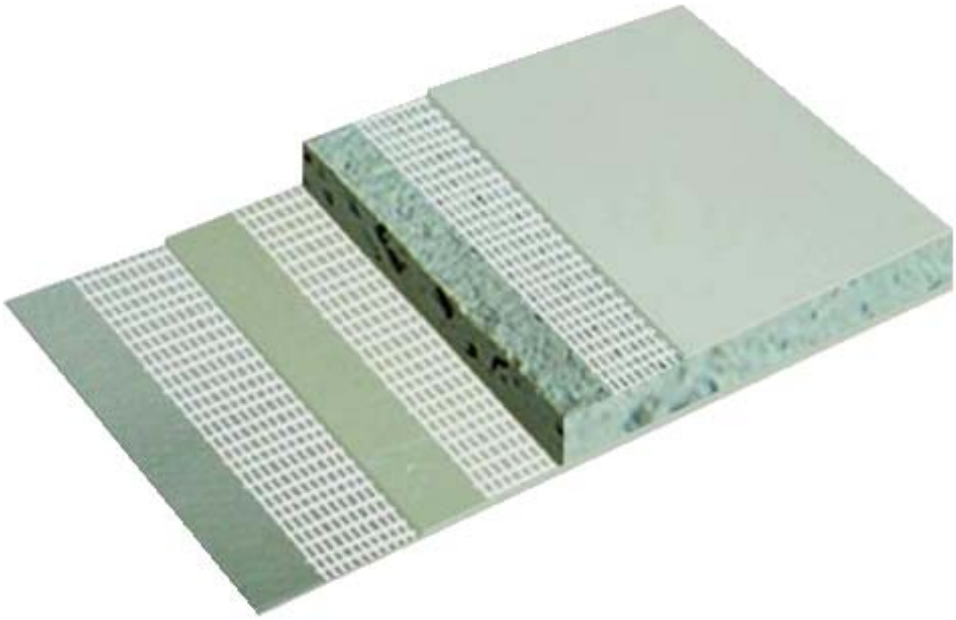

FIGURE 2

a)

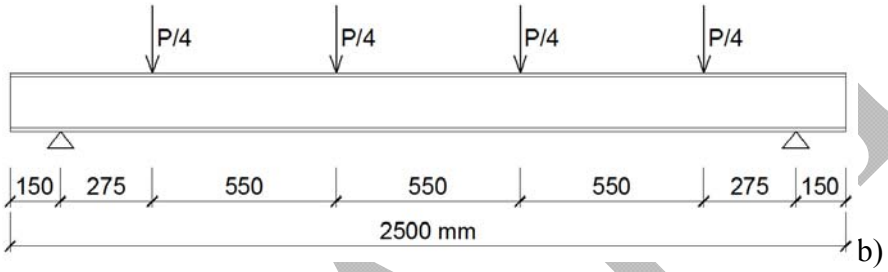

b)

FIGURE 3

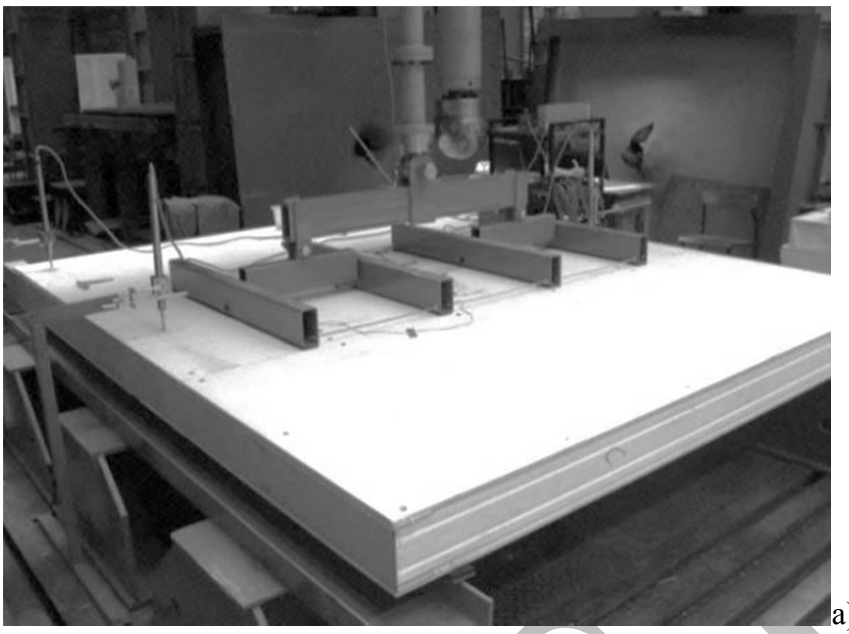

a)

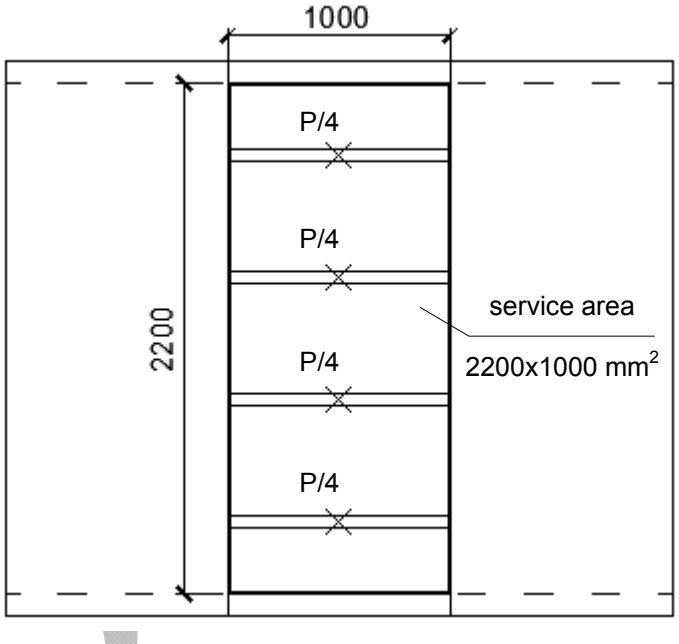

b)

FIGURE 4

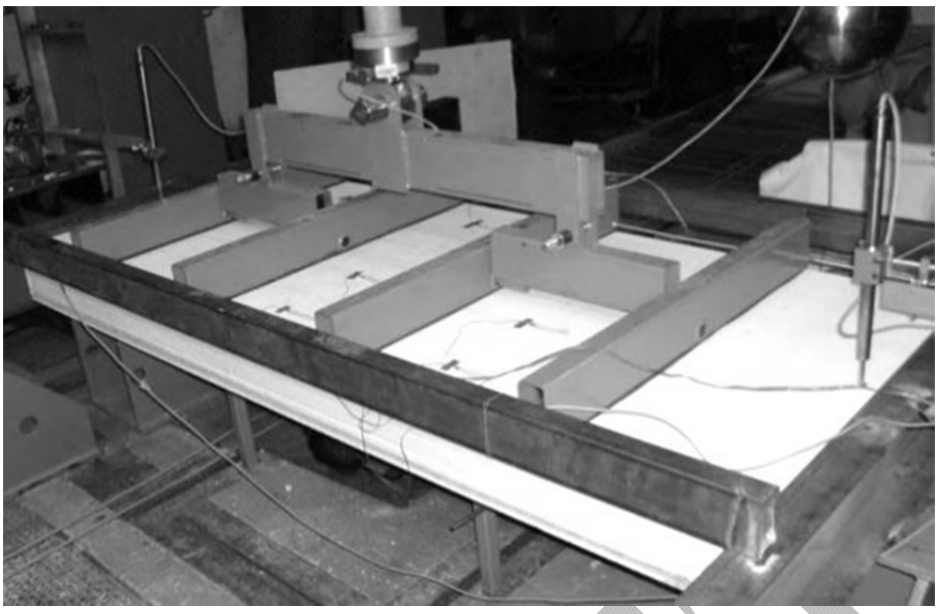

a)

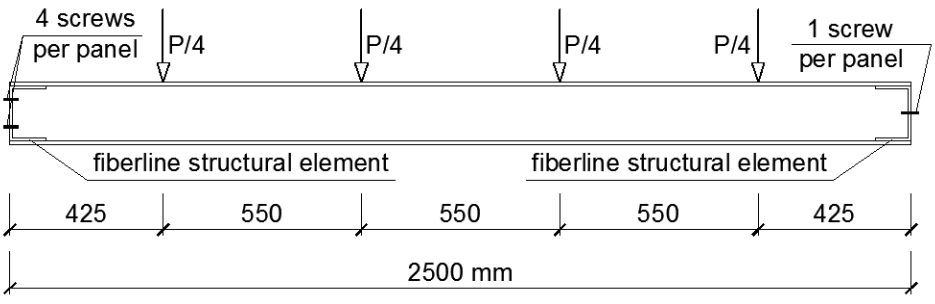

b)

FIGURE 5

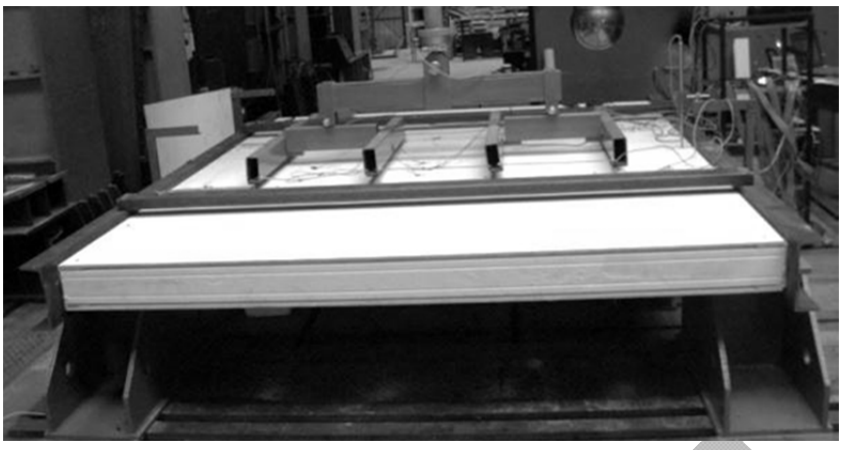

FIGURE 6

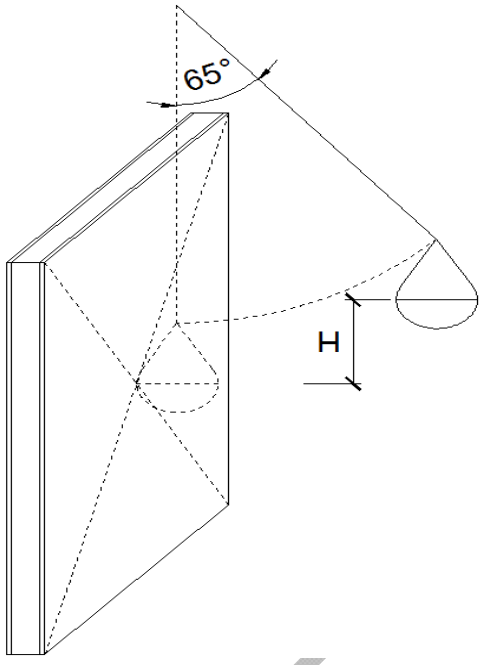

FIGURE 7

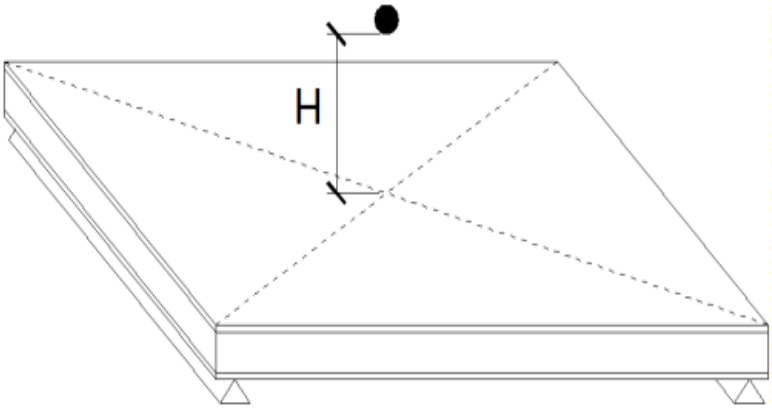

FIGURE 8

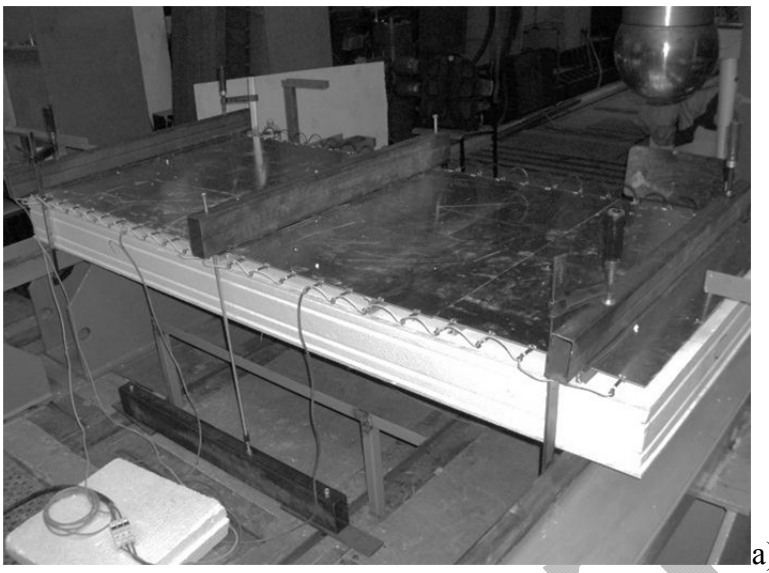

a)

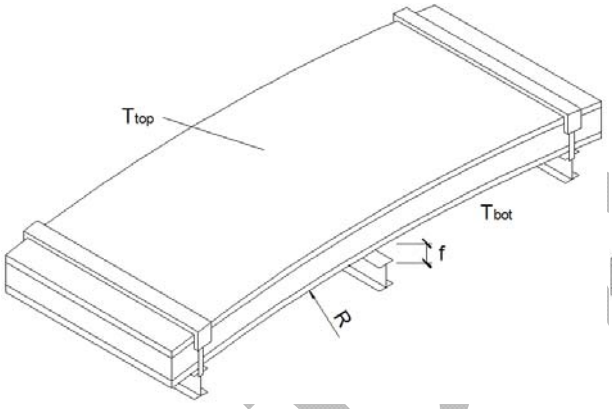

b)

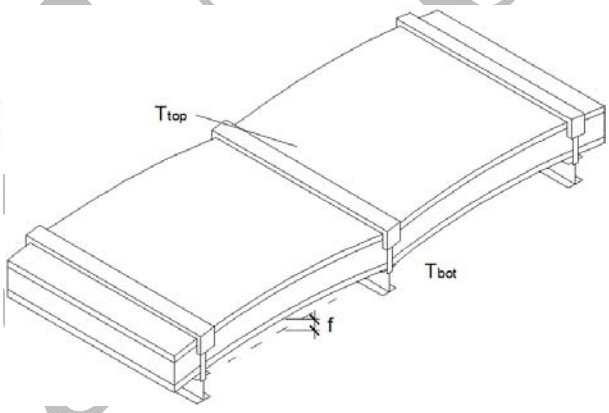

c)

FIGURE 9

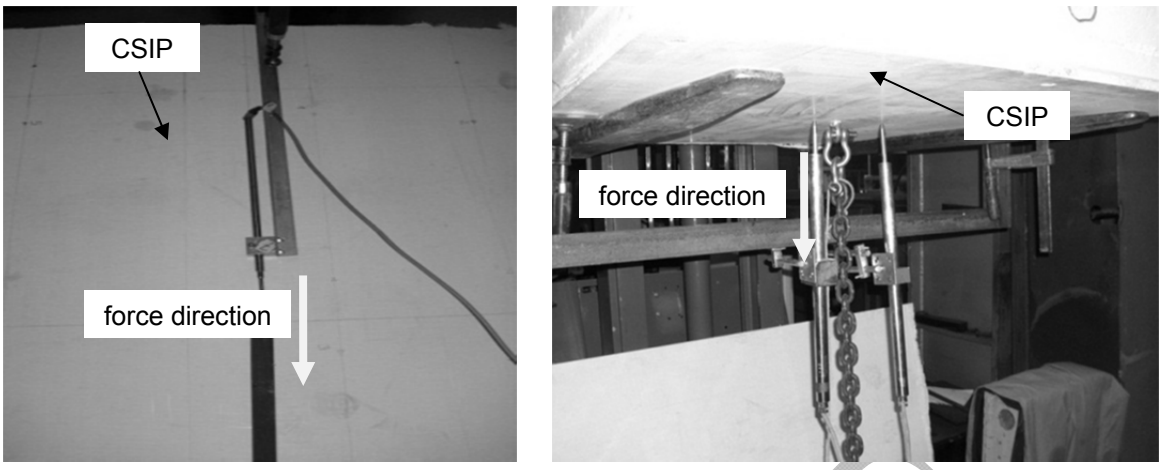

a) b)

FIGURE 10

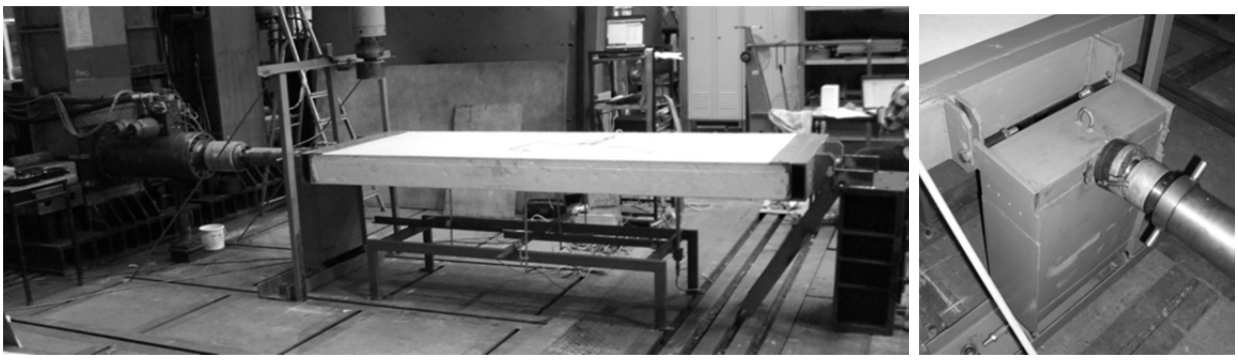

a) b)

FIGURE 11

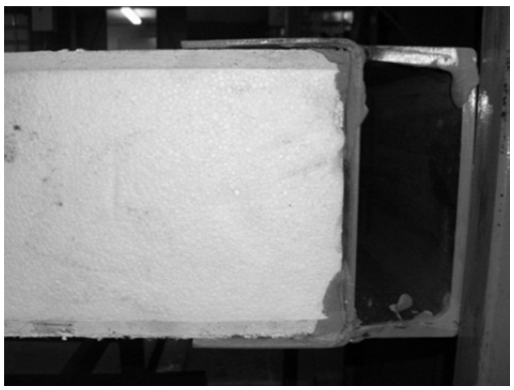

FIGURE 12

a) b) c)

FIGURE 13

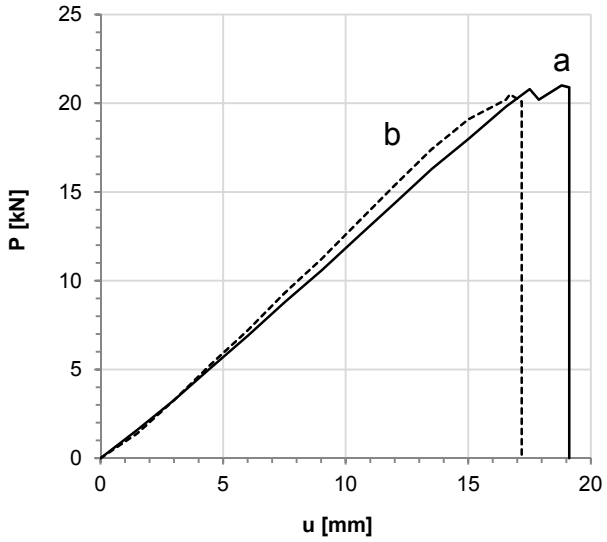

A)

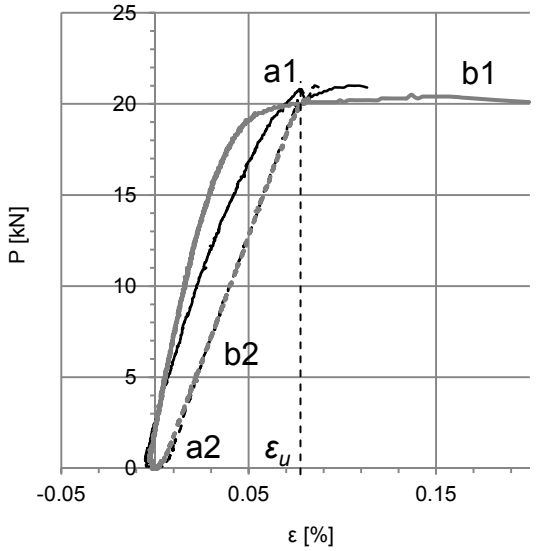

B)

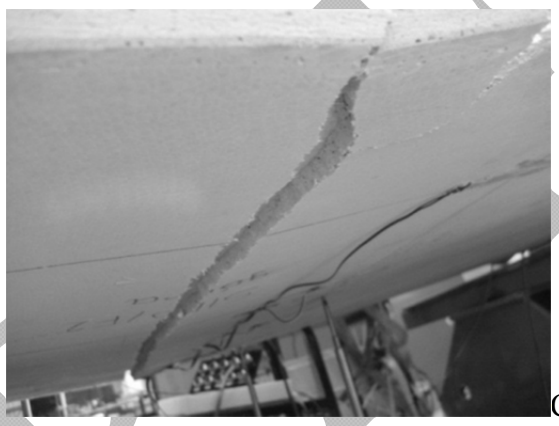

C)

I)

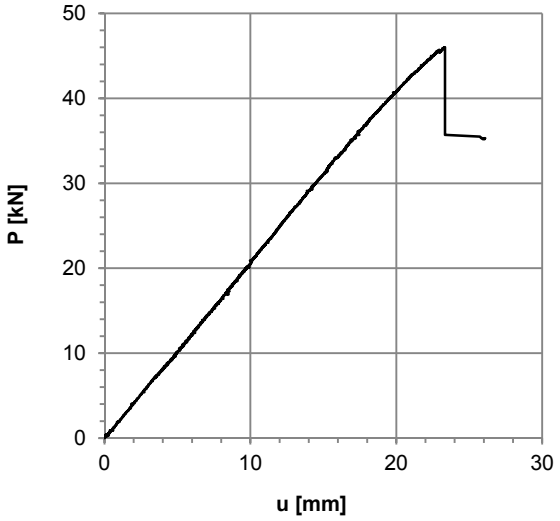

A)

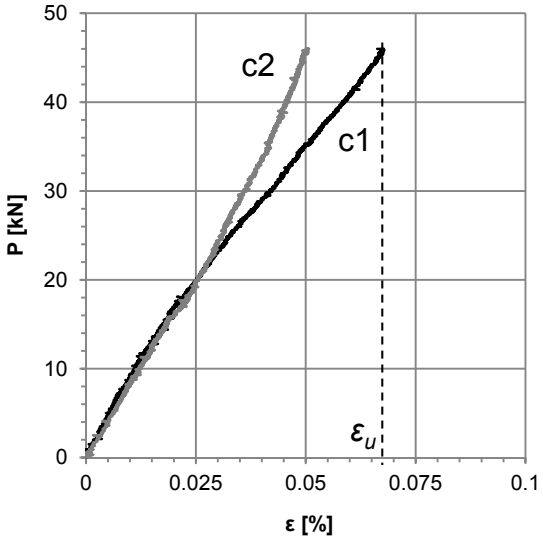

B)

C)

II)

FIGURE 14

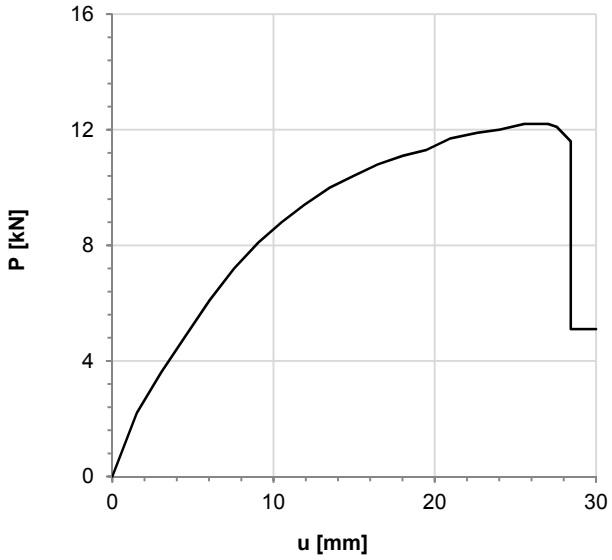

A)

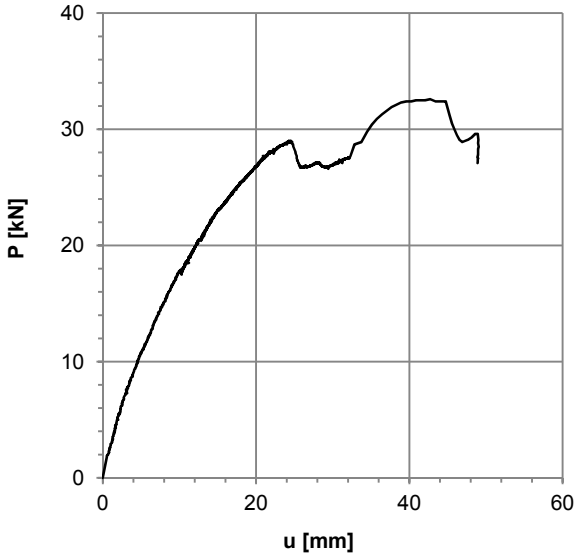

B)

FIGURE 15

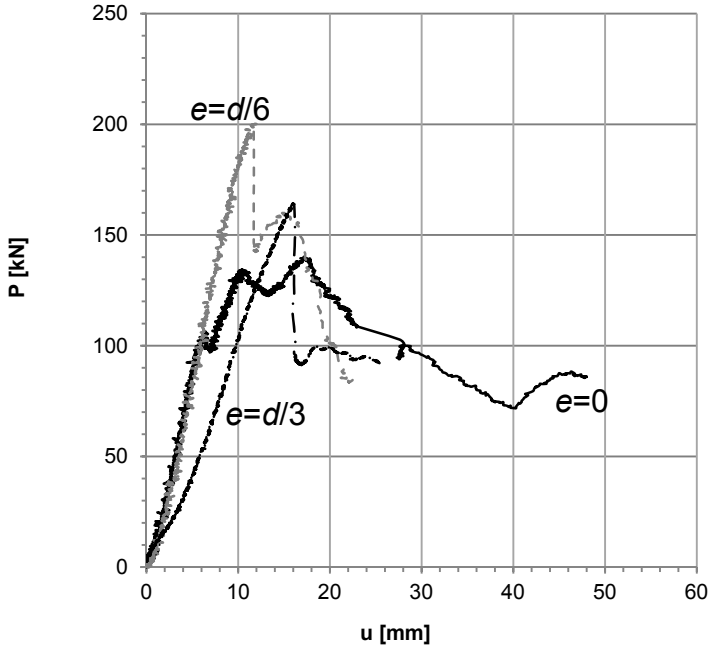

A)

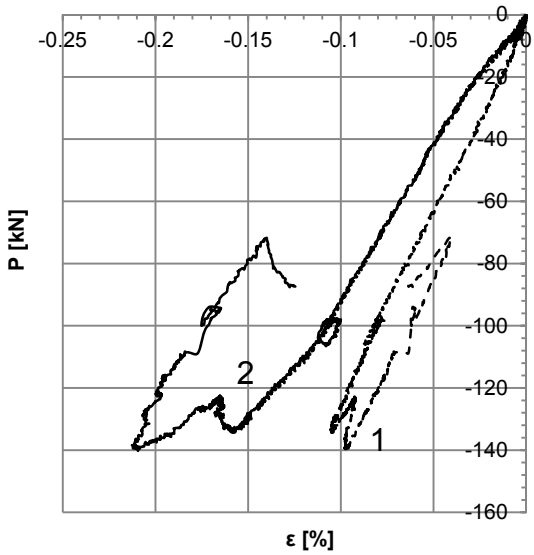

B)

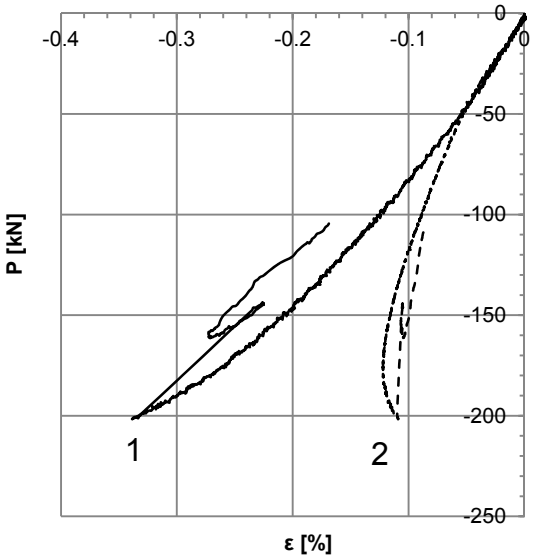

C)

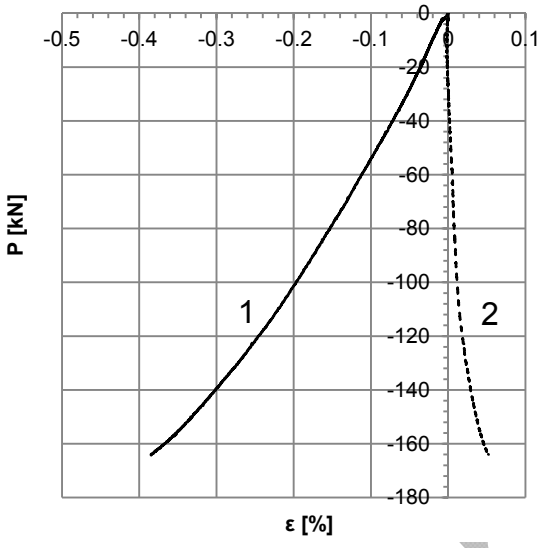

D)

FIGURE 16

a) b)

FIGURE 17

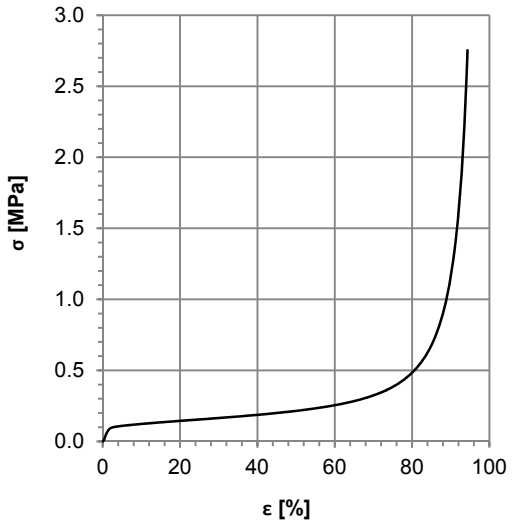

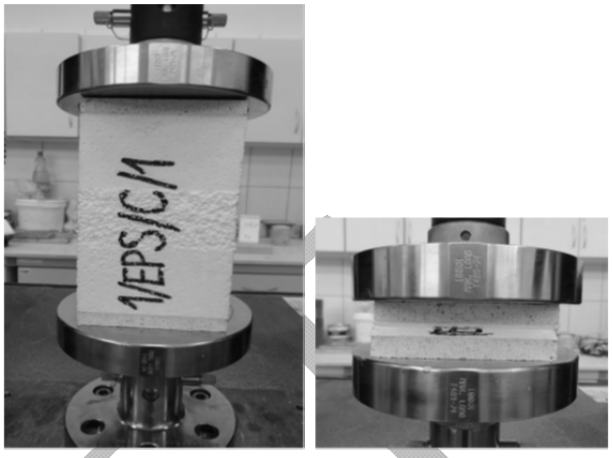

a) b)

A) B)

FIGURE 18

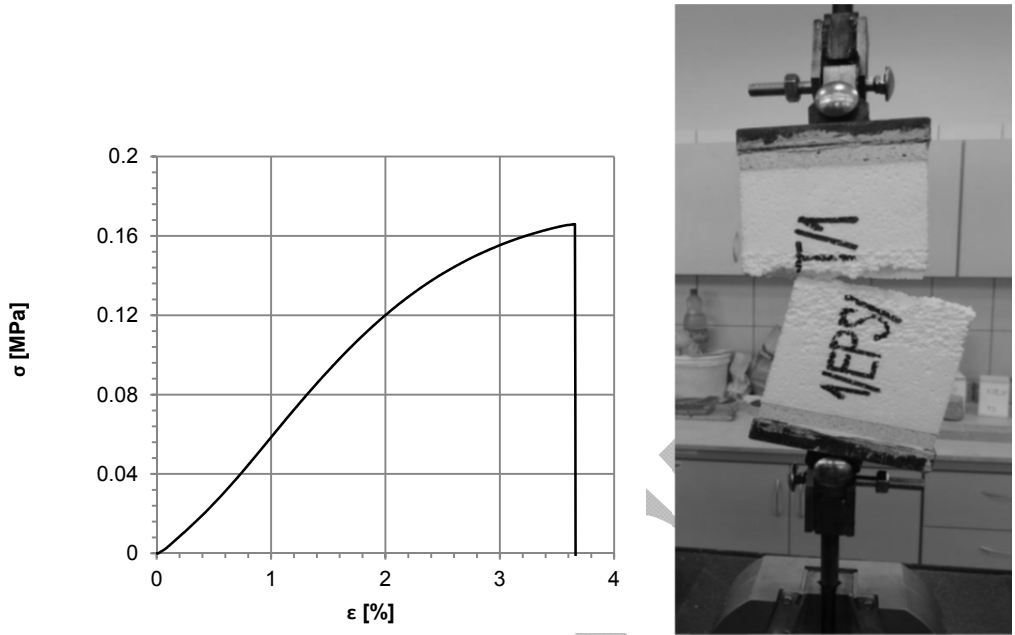

a) b)

FIGURE 19

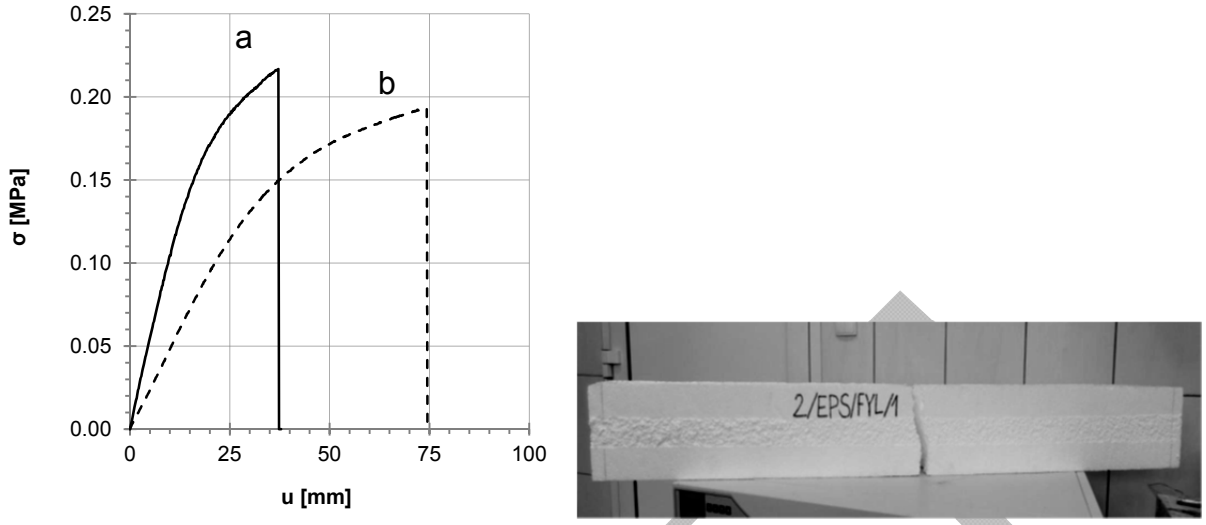

A) B)

FIGURE 20

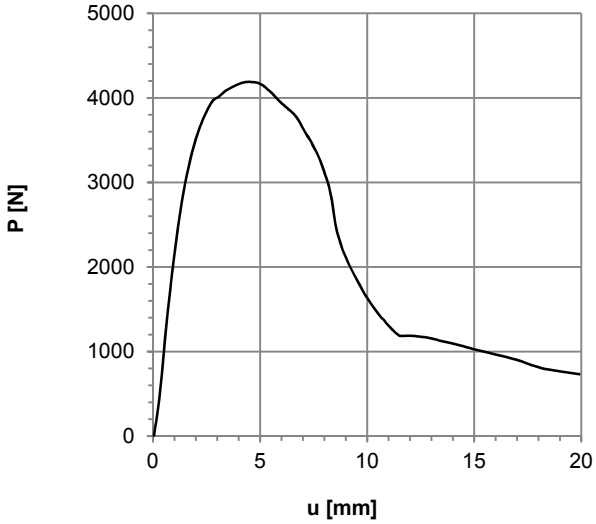

a)

b)

FIGURE 21

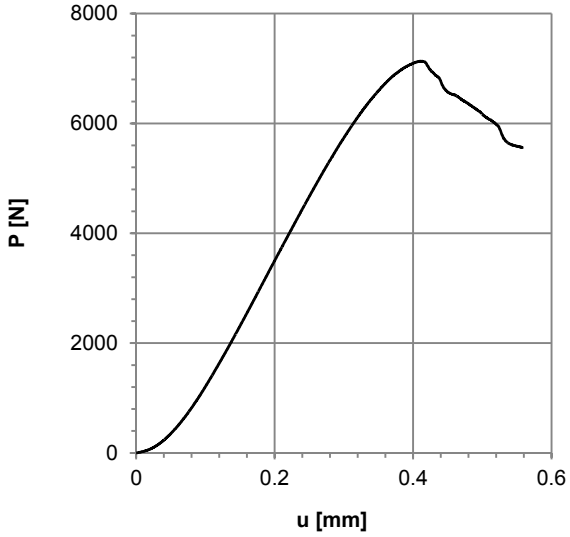

a)

b)

FIGURE 22

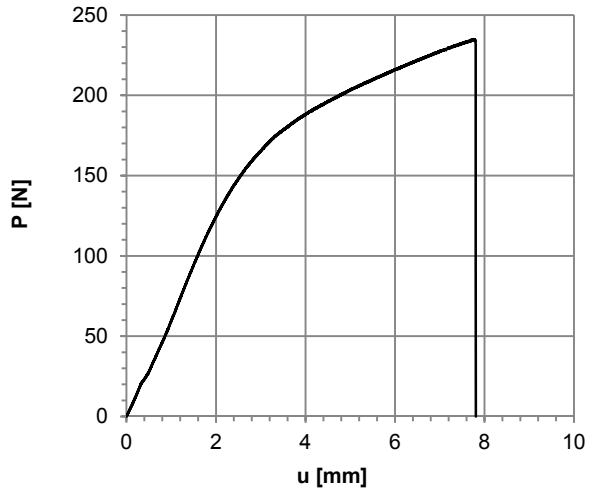

a)

b)

FIGURE 23

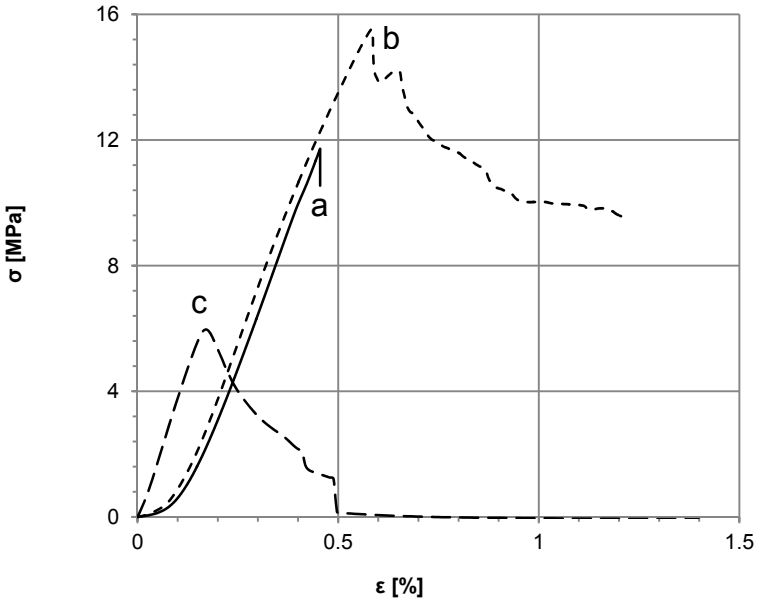

A)

a) b) c)

B)

FIGURE 24

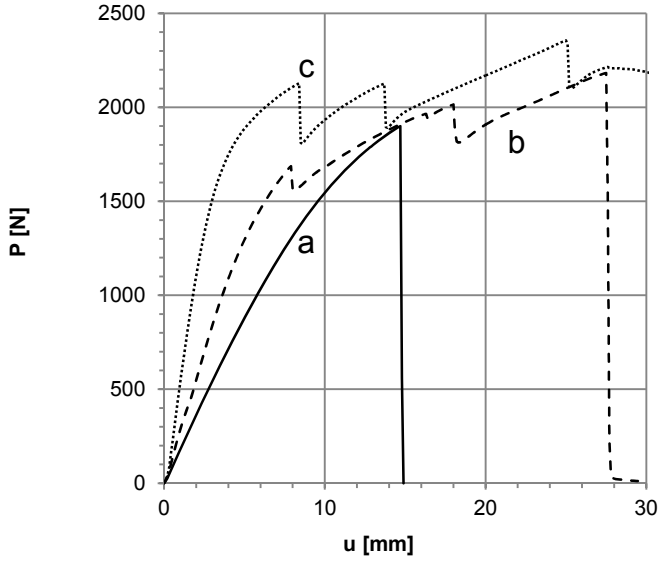

A)

a)

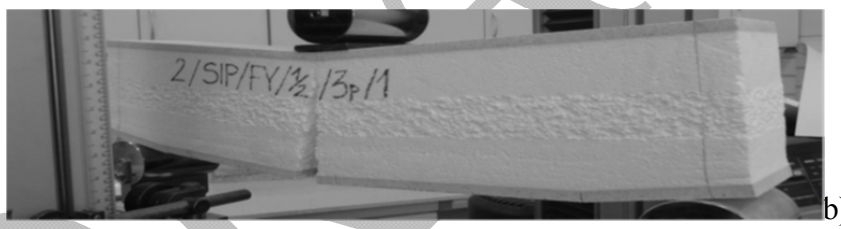

b)

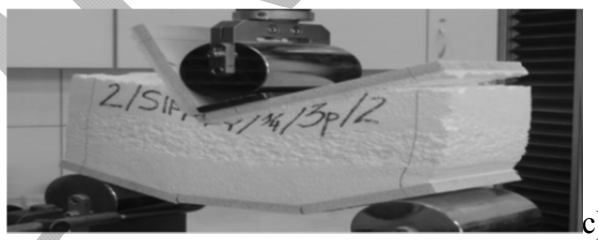

c)

B)

FIGURE 25

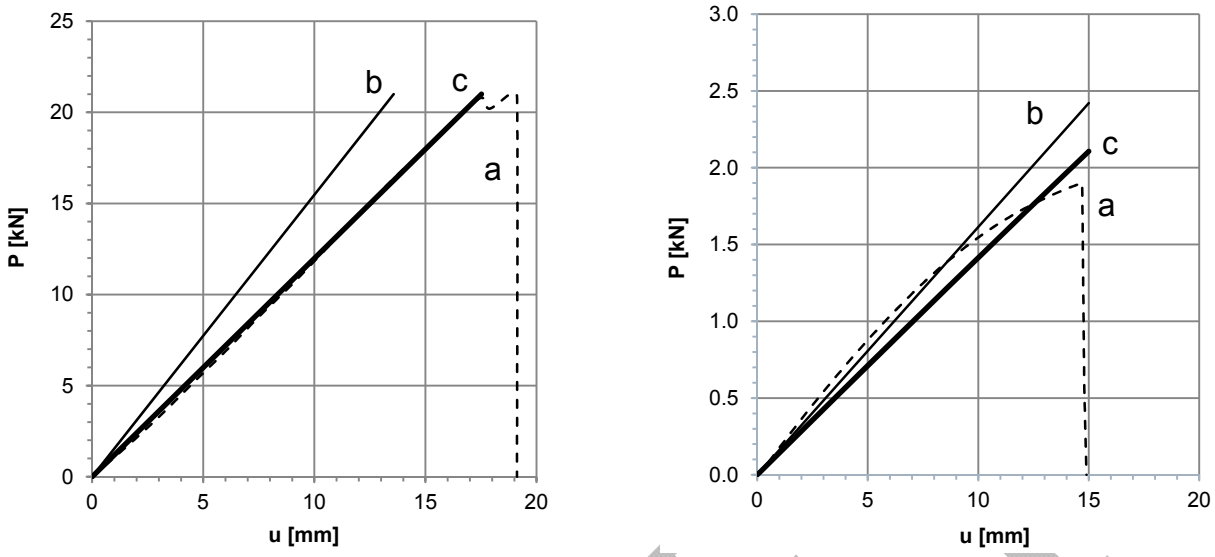

FIGURE 26

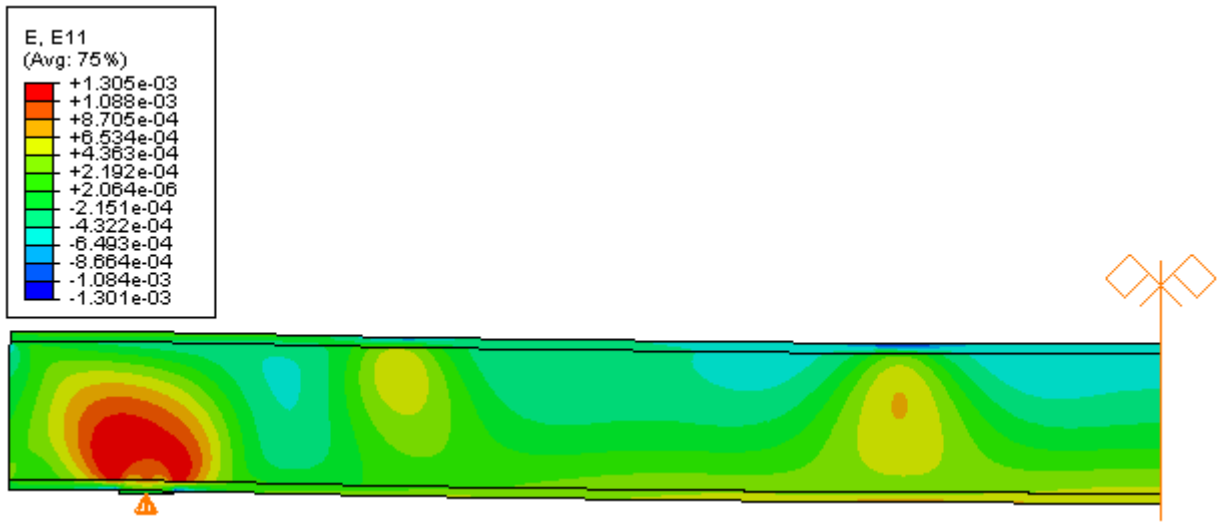

a)

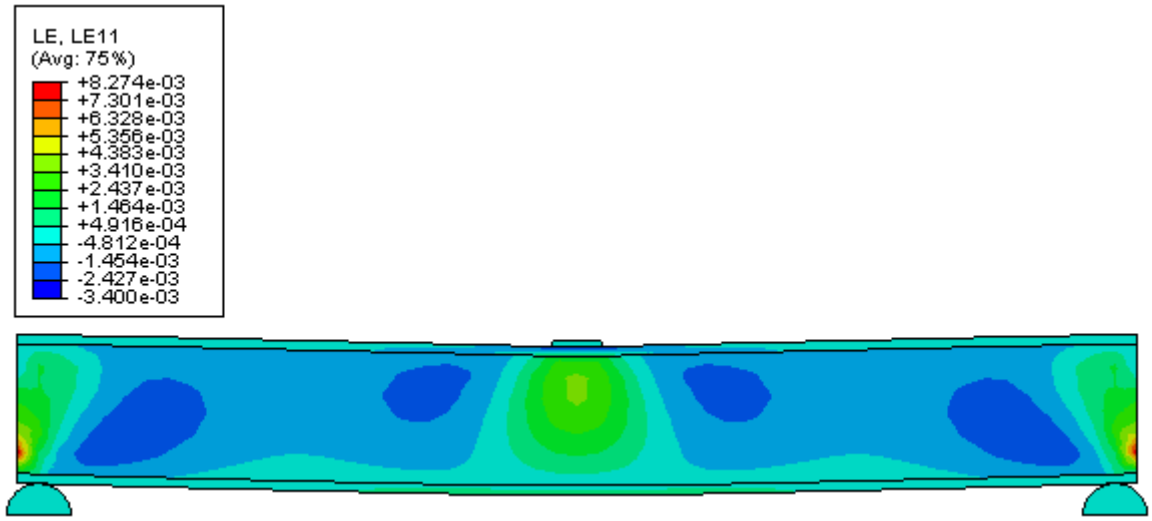

b)

FIGURE 27

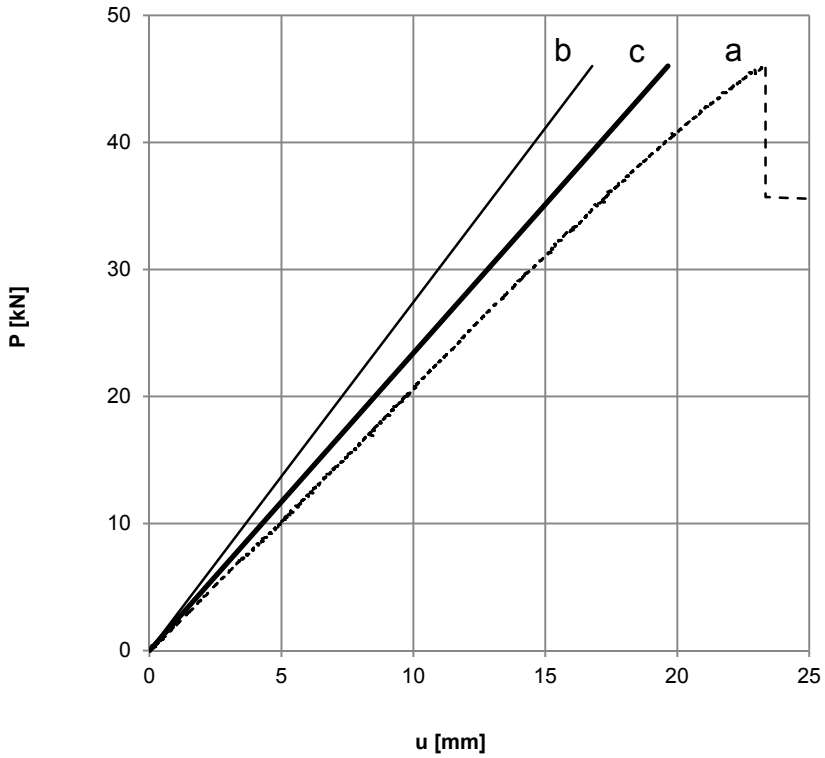

FIGURE 28

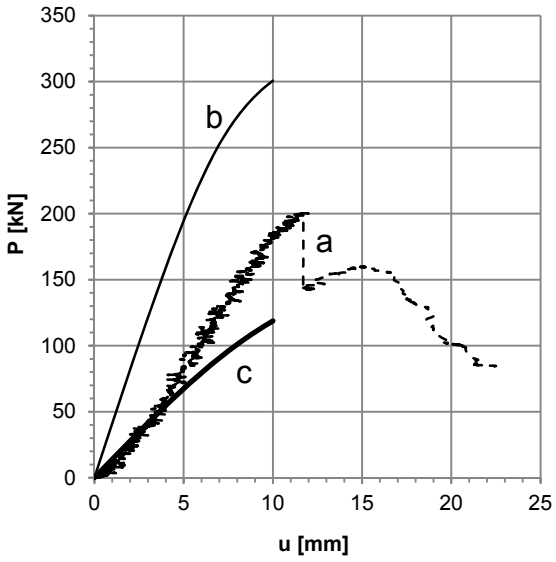

A)

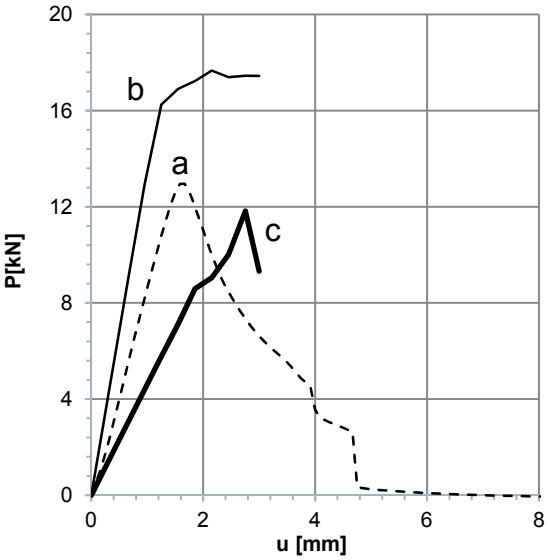

B)

FIGURE 29

LIST OF TABLES

Table 1: Test types and specimens used in large-scale experiments

Test type	Specimen type	Specimen size height×width×thick-ness[mm^3]	Support span [mm]
single free supported panel under bending	wall panel	2500×1000×174	2200
free supported 3-panels' wall under bending	3-panels' wall connected by OSB splines	2500×3000×174	2200
single panel on screws under bending	wall panel	2500×1000×174	2500
3-panel's wall supported on screws under bending	3-panels' wall connected by OSB splines	2500×3000×174	2500
soft body impact	3-panels' wall connected by OSB splines	2500×3000×174	2500
hard body impact	wall panel	2500×1000×174	2200
thermal test	wall panel	2500×1000×174	2500 (1st phase) 1250 (2nd phase)
single panel under compression	wall panel	2750×1000×174	3080

Table 2: Test types and specimens used in small-scale experiments

Test type	Material	Specimen size height×width×thickness [mm^3]	Support span [mm]
Flatwise compression and tension of expanded polystyrene	EPS	100×100×152	152
Expanded polystyrene under bending	EPS	1300×100×150 650×100×75	1250 600
Expanded polystyrene under shear	Doubled EPS	200×100×50	-
Edgewise compression of magnesia cement board	MgO board	50×50×11	50
Magnesia cement board under bending	MgO board	420×100×11	360
Edgewise compression of CSIP	CSIP	750×200×174 275×100×40 950×100×42	750 275 955
CSIP under bending	CSIP	325×100×174 650×100×174 1300×100×174	275 600 1250

Table 3: Mechanical properties of EPS core and magnesia cement facesheet from own and other laboratory tests [17]-[21] (E – modulus of elasticity, G – shear modulus, σ_u - ultimate normal stress, τ_u - ultimate shear stress, $\sigma_{10\%}$ - normal stress at ε=10%)

Material	Compression [MPa]	Tension [MPa]	Bending [MPa]	Shear [MPa]
EPS foam (mass density 20 kg/m^3)	$\sigma_{10\%}$=0.10-0.12 $\sigma_{10\%,avr}$=0.11 E=4.9-7.26 E_{avr}=6.09	σ_u=0.21-0.23 $\sigma_{u,avr}$=0.22 E=9.96-10.68 E_{avr}=10.37	σ_u=0.17-0.22 $\sigma_{u,var}$=0.20 E=7.27-8.47 E_{avr}=8.01	τ_u=0.21-0.23 $\tau_{u,avr}$=0.22 G=2.14-2.89 G_{avr}=2.51
EPS foam (mass density 20 kg/m^3) according to [17]-[20]	$\sigma_{10\%}$=0.11-0.12 E=5.6-6.3	σ_u=0.23-0.24 E=9.83-9.91	-	τ_u=0.07-0.11 G=2.44-2.74
Magnesia cement board (mass density 940 kg/m^3) production line direction	σ_u=10.63-18.28 $\sigma_{u,avr}$=13.50 E=1453-2610 E_{avr}=1922	-	σ_u=8.20-12.0 $\sigma_{u,avr}$=9.67 E=3458-8067 E_{avr}=5716	-
Magnesia cement board (mass density 940 kg/m^3) direction perpendicular to production line	σ_u=8.36-16.07 $\sigma_{u,var}$=13.10 E=1012-2384 E_{var}=1846	-	σ_u=6.02-7.91 $\sigma_{u,avr}$=7.03 E=4536-7497 E_{avr}=5611	-
Magnesia cement board according to [21]	σ_u=20.75	-	σ_u=8.9 E=6412	-